Chapter 8B. Analysis of Imaging Spectrometer Data for the Katawas Area of Interest

By Trude V.V. King and Michaela R. Johnson

Abstract

Computer analysis of the HyMap spectroscopic data of the Katawas area of interest (AOI) in the east-central part of Afghanistan used spectrum matching techniques to identify the occurrence of selected materials at the surface based on characteristic absorption features (absorption bands) in the HyMap data compared to a library of spectral standards. Although there are no known mineral occurrences in the AOI, several areas warranting additional studies are recognized.

Iron (Fe^{2+})-bearing minerals, chlorite or epidotes, and calcite and calcite mixtures dominate the AOI. The area has three potential areas that, based on the HyMap data, suggest areas with potential epithermal mineralization.

A northeast-trending, fault-bounded linear feature bisects the area, and mineralization occurs along and adjacent to the linear feature and an associated northeast-trending ridge. Minerals along and adjacent to the linear feature include epidote and chlorites, calcite and calcite mineral mixtures, serpentines, and Fe-bearing carbonates. Well-defined clusters of Fe^{3+}-bearing minerals are also present in the fault-bounded area.

The southern part of the fault-bounded area is characterized by carbonates, epidotes and chlorites, and smaller amounts of Fe-bearing carbonates that are seemingly bedded and lithologically controlled. In the northwestern part of the AOI, complex terrain that appears to be folded is characterized by calcite, epidotes or chlorites, and Fe-bearing carbonates, suggesting possible hydrothermal activity.

The presence of a known geochemical mercury anomaly (Peters and others, 2007) and the mapped mineral assemblages make this a very attractive area for future detailed exploration.

8B.1 Introduction

Previous U.S. Geological Survey (USGS) analyses of existing geologic data of Afghanistan revealed numerous areas with indications of potential mineral resources of various types (Peters and others, 2007). From these areas of interest, several were selected for follow-on studies using modern imaging spectrometer remote sensing data to further characterize surface materials. One of those areas is the Katawas area of interest (AOI) in east-central Afghanistan.

The Katawas AOI is approximately 150 km south-southwest of Kabul (fig. 8B–1) and is believed to have the potential for hot-springs gold, mercury, and base-metal deposits. To help assess these potential resources, high-resolution imaging spectrometer data were analyzed to detect the presence of selected minerals that may be indicative of past mineralization processes. This report contains the results of those analyses for the main Katawas AOI and the Katawas gold subarea. Katawas gold subarea mineral maps are subsets extracted from the same data as the Katawas AOI maps, but are presented at a larger scale, thus showing the mineral distribution patterns in more detail. Within the Katawas area, two areas deserving further investigation, especially detailed geological mapping and geochemical studies, are highlighted in King, Johnson, and others (2011).

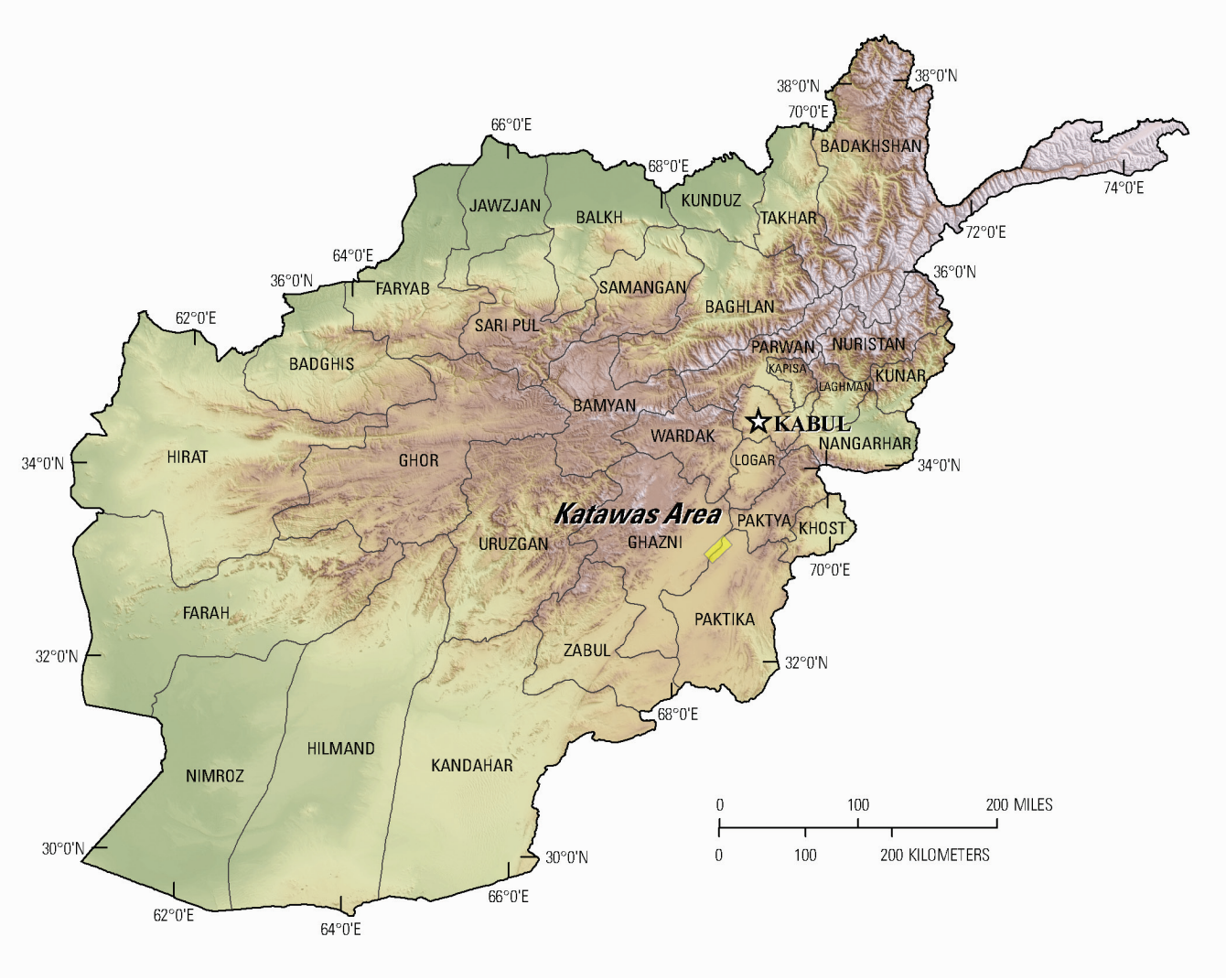

Figure 8B–1. The Katawas area of interest is located about 150 km south of Kabul in the Ghazni and Paktika Provinces and is believed to have the potential for hot-springs gold, mercury, and base-metal deposits.

8B.1.1 Imaging Spectrometer Data Collection and Processing

In 2007, imaging spectrometer remote sensing data were acquired over most of Afghanistan with the HyMap imaging spectrometer (Cocks and others, 1998), as part of the USGS Oil and Gas Resources Assessment of the Katawas and Helmand Basins project (Kokaly and others, 2008). These data were acquired from August 22, 2007 to October 2, 2007. There were 207 north-south flight lines and 11 cross-cutting calibration lines collected over Afghanistan, for a total of 218 flight lines covering a surface area of 438,012 km^2 (Kokaly and others, 2008). These data provide a means for characterizing surface materials in support of assessments of resources (coal, water, minerals, and oil and gas) and earthquake hazards in the country. Imaging spectrometers measure the reflectance of visible and near-infrared light from the Earth's surface in many narrow channels, producing a reflectance spectrum for each image pixel. These reflectance spectra can be interpreted to identify specific chemical transitions and molecular bonds that provide compositional information about specific materials occurring at the surface. The imaging spectrometer sensor data can only be used to characterize the upper surface materials and not subsurface composition or structure.

After undergoing a complex and rigorous data calibration process, the georeferenced and calibrated reflectance data were processed. The reflectance spectrum of each pixel of HyMap data was compared to the spectral features of reference entries in a spectral library of minerals, vegetation, water,

and other materials (King, Kokaly, and others, 2011; Kokaly and others, 2011). The best spectral matches were determined, and the results were clustered into classes of materials discussed below.

8B.1.2 Calibration Process

To ensure the utility of the imaging spectrometer dataset, a rigorous calibration process to remove atmospheric absorptions and residual instrument artifacts was applied. Before the calibration process started, each flight line was georeferenced to Landsat base imagery in UTM projection (Davis, 2007). Because of the extreme topographic relief and restricted access to ground-calibration sites, modifications to the traditional USGS calibration procedures were required to calibrate the 2007 Afghanistan HyMap dataset (Hoefen and others, 2010). Radiance data were converted to apparent surface reflectance using the radiative transfer correction program Atmospheric CORrection Now (ACORN; ImSpec LLC, Palmdale, Calif.). ACORN was run multiple times for each flight line, using average elevations in 100-m increments, covering the range of minimum to maximum elevation within the flight line. A single atmospherically corrected dataset was assembled from the ACORN results in 100-m increments. This was done by determining the elevation of each pixel and selecting the atmospherically corrected pixel from the 100-m increment closest to the elevation of the pixel. The atmospherically corrected dataset was further empirically adjusted using ground-based reflectance measurements from the Kandahar Air Field, Bagram Air Base, and Mazar-e-Sharif Airport, as well as soil samples from two fallow fields. To improve the data quality, new calibration techniques were developed to address the atmospheric differences within a flight line.

To refine data quality of ground-calibrated reflectance, a multiplier correction, computed by cross-calibrating north-south flight lines with a flight line that passed over a ground-calibration site, was applied. For each north-south flight line, the pixels in overlap regions of north-south and cross-cutting calibration lines, subject to slope, vegetation cover, and other restrictions, were used to develop these cross-calibration correction factors (Hoefen and others, 2010). The cross-calibration multiplier corrected any residual atmospheric contamination in the imaging spectrometer data that was not present in the spectra of the ground-calibration site.

8B.1.3 Materials Maps and Presentation

HyMap reflectance data were processed using Material Identification and Characterization Algorithm (MICA), a module of the U.S. Geological Survey Processing Routines in Interactive Data Language (IDL) for Spectroscopic Measurements (PRISM) software (Kokaly, 2011). MICA compared the reflectance spectrum of each pixel of HyMap data against entries in a reference spectral library of minerals, vegetation, water, and other materials. The library included 97 reference spectra of well-characterized mineral and material standards. The resulting maps of material distribution, resampled to a 23×23 m^2 pixel grid, were used to prepare maps of mineral, vegetation, and other material occurrences.

HyMap data were analyzed twice. MICA was first run using the set of minerals with absorption features in the visible and near-infrared wavelength region, producing the 1-micron (µm) map of iron-bearing minerals and other materials (King, Kokaly, and others, 2011). MICA was run again using the minerals with absorption features in the shortwave infrared, producing the 2-µm map of carbonates, phyllosilicates, sulfates, altered minerals, and other materials. For clarity of presentation, some individual classes in these two maps were bundled by combining selected specific mineral types (for example kaolinites, montmorillonites, and hematites) to reduce the number of mineral classes. The iron-bearing minerals map has 27 classes. Iron-bearing minerals with different mineral compositions but similar spectral features are difficult to classify as specific mineral species. Thus, generic spectral classes, including several minerals with similar absorption features, such as Fe^{3+} Type 1 and Fe^{3+} Type 2, are depicted on the map. The carbonate, phyllosilicates, sulfates, and altered minerals map has 31 classes. Minerals with slightly different mineral compositions but similar spectral features are less easily discriminated; thus, some identified classes consist of several minerals with similar spectra,

such as the chlorite or epidote class. When comparisons with reference spectra produced no viable match, a designation of "not classified" was assigned to a pixel.

Although the occurrence of certain minerals (pyrophyllite, buddingtonite, dickite, and jarosite) may suggest that mineralization processes may have once operated in the area, many of the minerals that were identified are also common rock-forming minerals. Consequently, the distribution patterns of the identified minerals are extremely important in understanding the causes of mapped mineral occurrences and evaluating the possible potential for related mineral deposits.

8B.1.4 Data Limitations

It should be noted that geographic registration between various datasets is not always possible, because of differences in collection methods and resolution. The geographic accuracy and quality of each dataset is limited by the original source. Significant efforts were made to ensure the geographic accuracy of the HyMap data (Kokaly and others, 2008; Hoefen and others, 2010). However, exact registration between previously published known mineral occurrences, fault traces, geologic units, and structural boundaries in comparison to the HyMap data may not be ideal. To resolve additional details, the digital versions of these maps can be viewed at higher spatial resolution than what is possible in a single-page printed map.

8B.2 Geologic Setting of the Katawas Area of Interest

The Katawas hot-springs gold, mercury, and base-metals deposits are located in the Ghazni and Paktika Provinces of Afghanistan (fig. 8B–1). The Katawas AOI is approximately 478 km^2 and the Katawas gold subarea is approximately 143 km^2. The elevation in the AOI ranges from 2,079 to 3,052 m (fig. 8B–2). High northeast-trending terrain dominates the central portion of the AOI, and lower terrain occurs in the northern, northeastern, and western parts. Landsat Enhanced Thematic Mapper (TM) data for the AOI (fig 8B–3) show that the rocks range from light colors to greenish, red, and black. Two subparallel faults that strike southwest to northeast extend three-quarters of the extent of the AOI, and rocks range in age from Paleocene to Recent (fig. 8B–4). Small cultivated plots of land and a lake occur in the northern part of the AOI.

8B.3 Imaging Spectrometer Material Maps of the Katawas Area of Interest

Spectroscopic analysis of the HyMap imaging spectrometer data of the Katawas AOI resulted in the identification of a variety of surficial minerals. These minerals have been identified by the presence and wavelength position of absorption features in the 0.45–2.48 μm wavelength. Two general categories of minerals are recognized: (1) iron-bearing minerals that have characteristic spectral absorption features that occur at wavelengths near 1 μm, and (2) a wide variety of minerals, including carbonate, mica, and clay minerals, and sulphates that have diagnostic spectral absorptions near 2-μm wavelength. Although the occurrence of certain minerals may suggest mineralization processes may have operated in the area, many of the minerals identified and mapped are also common rock-forming minerals or minerals that can be derived from the weathering of a variety of rock types. Consequently, the distribution patterns of the identified minerals and the geologic content where they occur are extremely important in understanding the causes of the mapped mineral occurrences and assessing the potential for related mineral deposits.

A companion report and geodatabase of potential mineral resource anomalies (areas of potential economic mineral resource occurrence) that have not been previously recognized or where the HyMap data has expanded the geologic understanding of the prospect can be found in King, Johnson, and others (2011).

8B.3.1 Katawas Area of Interest

Figures 8B–5 and 8B–6 show the distribution of identified surficial minerals and other materials for the entire Katawas AOI. Figure 8B–5 shows the distribution of Fe-bearing minerals and other materials (28 possible classes), and figure 8B–6 shows the distribution of carbonates, phyllosilicates, sulphates, altered minerals, and other materials (32 possible classes). Because of the large number of mineral classes represented and the subtleties of the distribution patterns in these maps, it is more instructive to display these results as a series of topical images depicting a group of minerals that are commonly related or occur together in special geologic environments (figs. 8B–7 to 8B–11). Figure 8B–7 shows the distribution of carbonate minerals in the AOI; figure 8B–8 shows the distribution of clays and micas; figure 8B–9 shows the distribution of iron oxide and hydroxide minerals; figure 8B–10 shows the distribution of secondary minerals; and figure 8B–11 shows the distribution of minerals commonly found in hydrothermally altered rocks.

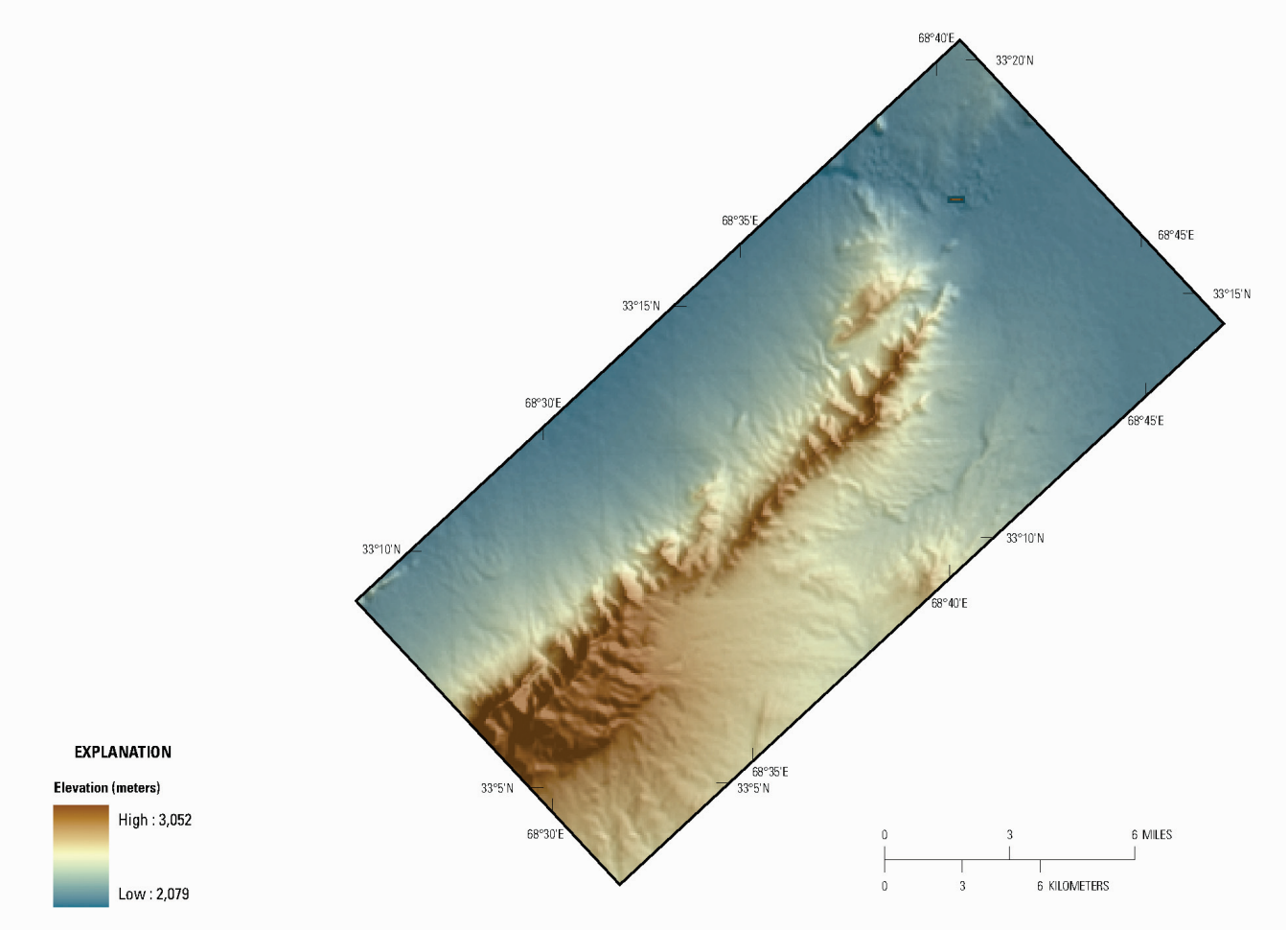

Figure 8B–2. Shaded relief map showing elevations in the Katawas area of interest (AOI). High northeast-trending terrain dominates the central portion of the AOI, and lower terrain occurs in the northern, northeastern, and western parts.

8B.3.1.1 Carbonate Minerals

The calcite and calcite + muscovite/illite mineral groups are the primary carbonate minerals in the AOI (fig. 8B–7). The calcite group minerals preferentially occur in the fault-bounded central portion of the area. A fewer number of dolomites and dolomite mixtures are present in the area and occur both in the southwest portion of the image (Paleocene rocks) and in the central fault-bounded area. A scattering of dolomitic minerals occur in the Eocene and Pliocene rocks on the east side of the central

fault-bounded area. In the northwestern part of the image, near lat 68°37′28.73″E., long 33°14′48.56″N., is an area that is free of calcite and montmorillonite mixtures, but exhibits well-defined distributions of calcite. A small Eocene unit on the northwest side of the AOI, adjacent to the boundary, is dominantly calcite, but also has minor amounts of calcite and montmorillonite. Fe-bearing carbonates occur along the length of the central fault-bounded region as well as along an east-northeast-trending ridge near lat 68°38′45″E., long 33°12′10″N. that originates within the central fault-bounded region.

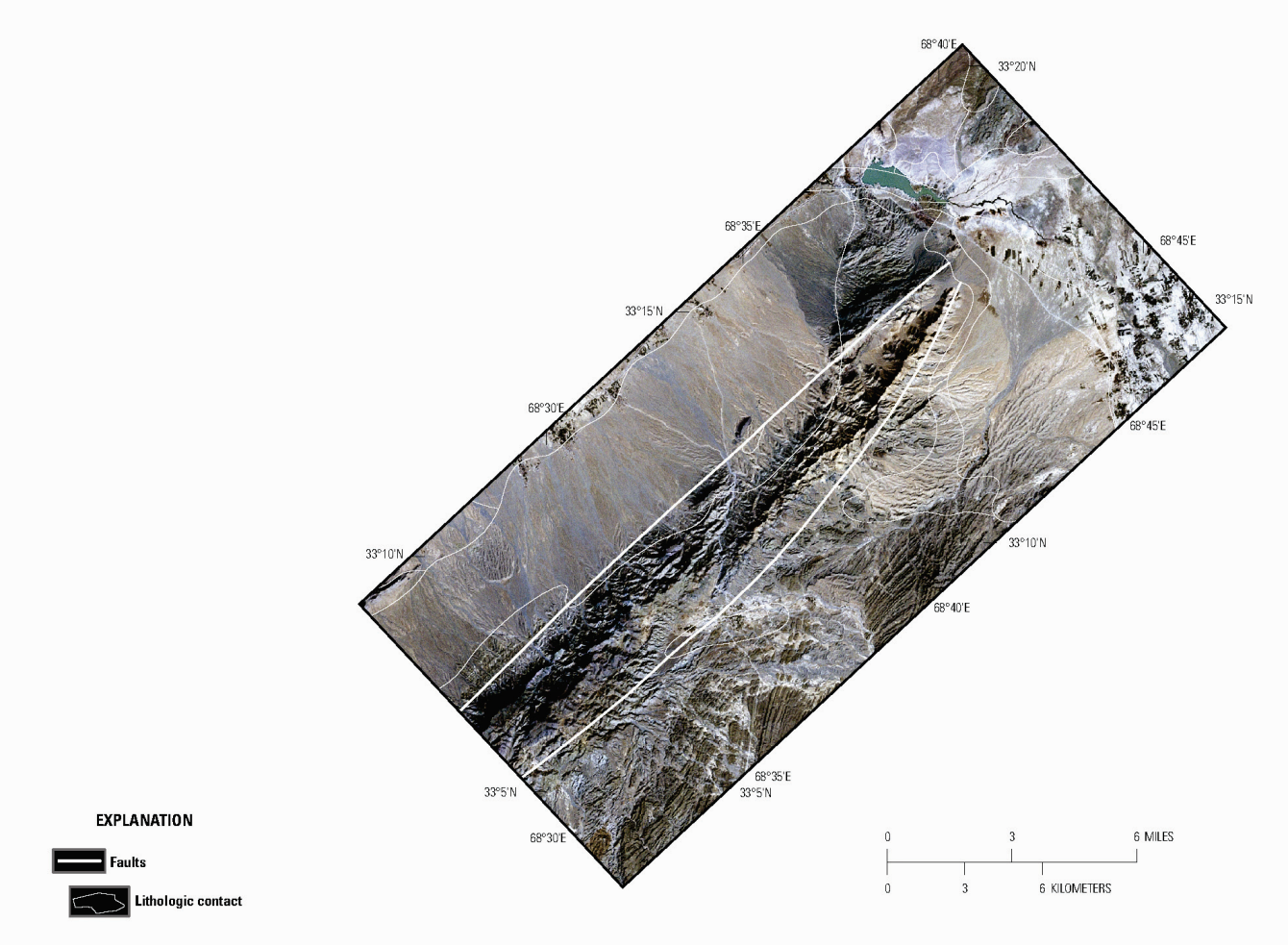

Figure 8B–3. Several northeast-striking faults occur in the Katawas area of interest. The Landsat Enhanced Thematic Mapper (TM) images show that the rocks range from light colors to greenish, red, and black. (Davis, 2007).

8B.3.1.2 Clays and Micas

The clays and micas are mapped in all ages of rocks within the AOI (fig 8B–8).

Muscovites and illites are the most abundant minerals. Pixels of chlorite and epidote and illitic minerals dominate the central fault-bounded area that cross-cuts the AOI. The portion of the AOI east of the central fault-bounded area is dominated by spatially coherent groups of illite and muscovite with lesser amounts of chlorite and epidote. The bedded rocks of Eocene age that appear in the "greenish" colored areas in the TM image of the AOI (fig 8B–3) are mapped as illite with lesser amounts of epidote and chlorite. Some illitic rocks occur in the northeast portion of the AOI in Pliocene, late Quaternary, and Recent rocks. Illite, muscovite, and chlorite and epidote occur in the southwestern portion of the AOI and appear to be eroded from the fault-bounded portion of the central ridge. Strong concentrations of chlorite or epidote and illite occur in the Eocene rocks in the area adjacent to the northern terminus of the central fault-bounded area near lat 68°37′28″E., long 33°14′48 ″N. These rocks appear dark in the

TM image and have a morphology commonly associated with extrusive rocks. Montmorillonite-rich surficial materials are present near lat 68°43′27″E., long 33°17′38″N., in Quaternary and Recent rocks.

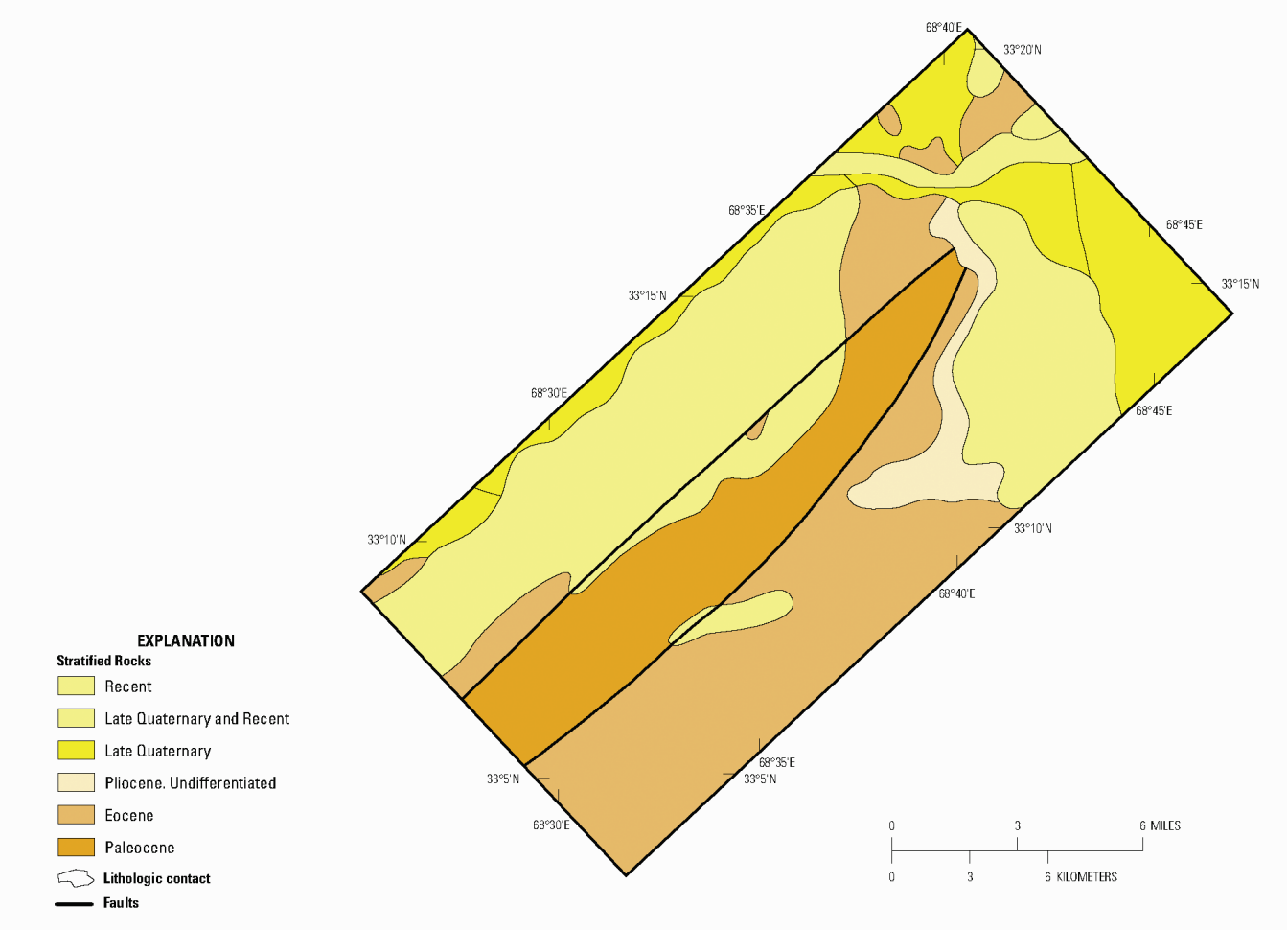

Figure 8B–4. Within the Katawas area of interest, the prominent faults strike southwest to northeast and rocks range in age from Paleocene to Recent. Geologic map is taken from Doebrich and others (2006).

8B.3.1.3 Iron Oxides and Hydroxides

Figure 8B–9 shows iron-bearing and other alteration minerals in the Katawas AOI. The central, fault-bounded region of the AOI primarily contains epidote with lesser amounts of goethite-bearing minerals and minor amounts of hematite associated with the east-northeast-trending ridge near lat 68°38′35″E., long 33°12′11″N. Chlorite or epidote pixels occur in the extrusive rocks near lat 68°38′29″E., long 33°14′48″N., and in the southern half of the AOI where chlorite or epidote is both lithologically controlled and represents erosional material of Paleocene, Eocene, and late Quaternary rocks (figs. 8B–6 and 8B–9).

8B.3.1.4 Common Secondary Minerals

The occurrence and distribution of common secondary minerals for the Katawas AOI are shown in figure 8B–10. The dominant secondary minerals in the AOI are epidote and the chlorite or epidote group. Pixels of epidote-bearing minerals are spatially distributed over the area as well as in spatially coherent clumps and part of intermingled mineral groups.

Serpentine pixels are present in the central, fault-bounded area as spatially coherent clusters between lat 68°34′50″E., long 33°9′57″N. and lat 68°38′47″E., long 33°12′9″N., in Eocene rocks.

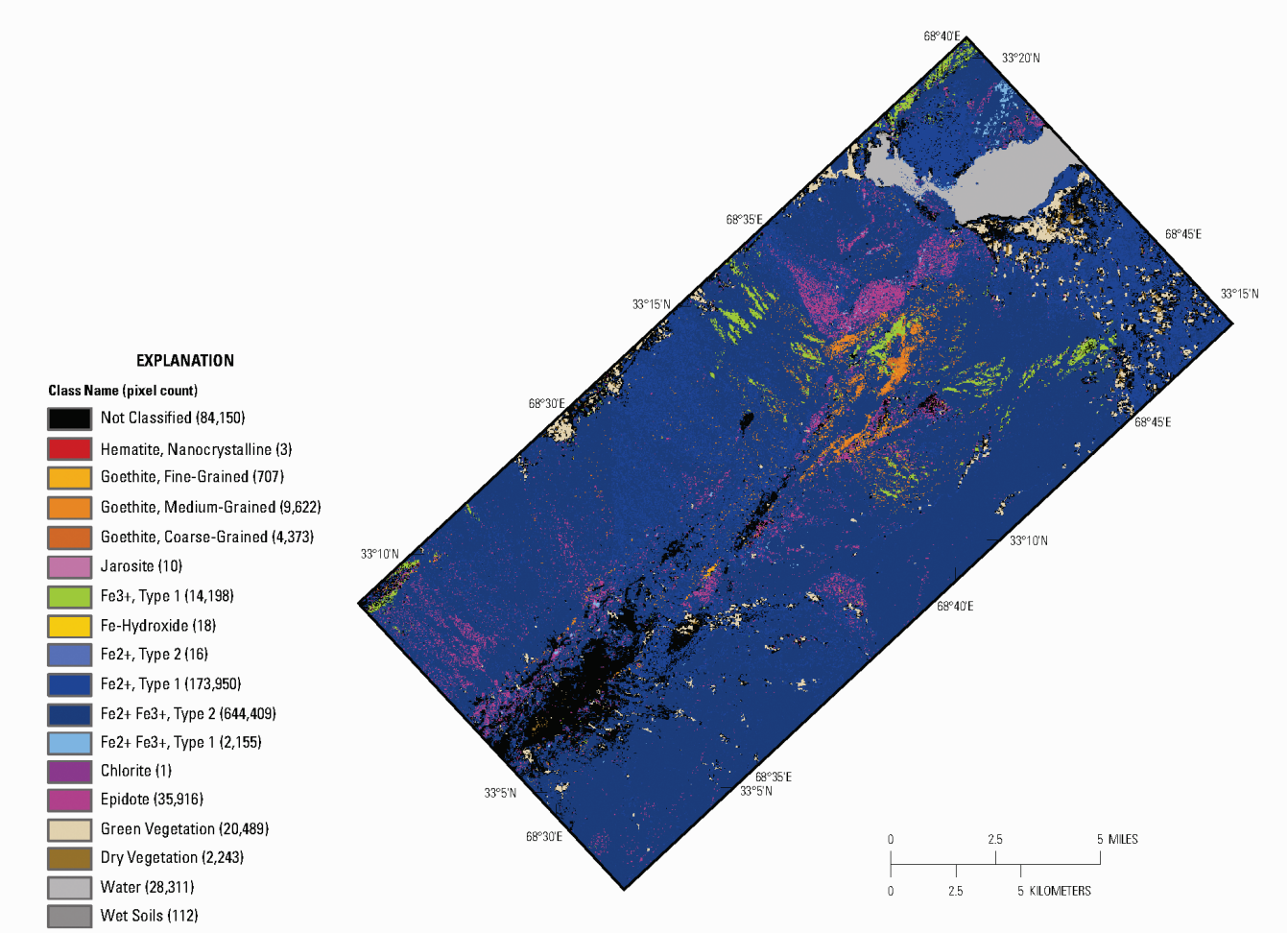

Figure 8B–5. Distribution of iron-bearing and other alteration minerals in the Katawas area of interest detected in the HyMap data.

8B.3.1.5 Common Alteration Minerals

Most of the minerals in this group are commonly present in hydrothermally altered rocks associated with epithermal processes. Consequently, where they occur in distinct clusters is of great interest in terms of potential mineral deposits. However, only chlorite or epidote group minerals and Fe-bearing carbonate minerals were mapped in the area (fig 8B–11).

8B.3.2 Katawas Gold Subarea

There are no known mineral occurrences in the Katawas gold subarea. The topography in the area ranges from 2,087 to 2,715 m. High terrain dominates the central portion and lower terrain occurs in the northern and northeast part of the subarea (fig. 8B–12). The surficial materials in the TM data (fig. 8B–13) show a range in colors including very light, red, greenish, and dark rocks. Small cultivated plots of land occur in the northern part of the AOI. The geologic map of the area (fig. 8B–14) shows rocks ranging from Paleocene to Recent that do not appear to be well correlated with the color variations shown in the TM data. Figures 8B–15 and 8B–16 show the distribution of carbonate, sulphate, phyllosilicate and other alteration minerals, and the distribution of Fe-bearing minerals in the subarea.

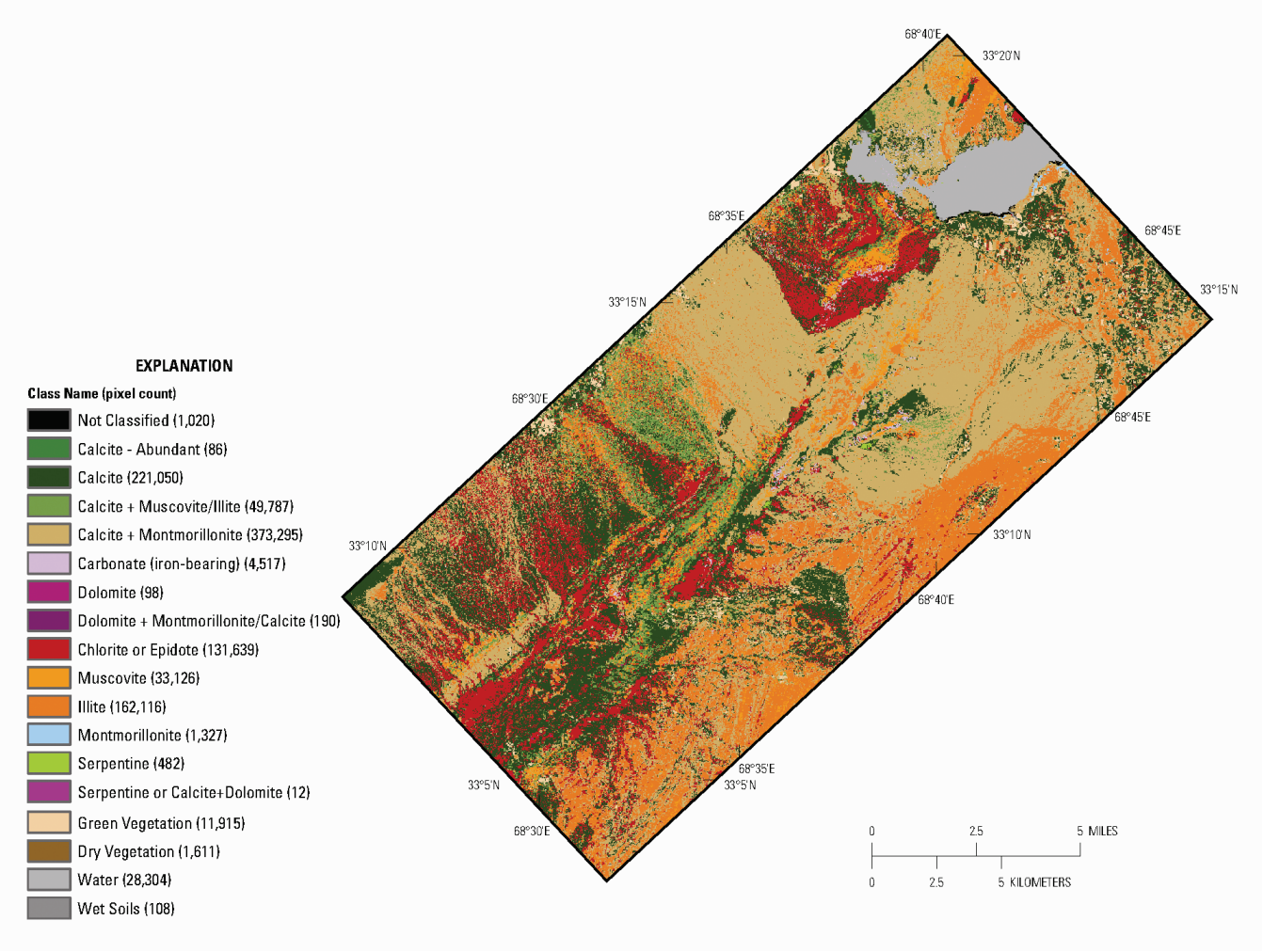

Figure 8B–6. Distribution of clays, carbonates, phyllosilicates, sulphates, and other alteration minerals for the entire Katawas area of interest detected in the HyMap data.

8B.3.2.1 Katawas Gold Subarea: Carbonate Minerals

The calcite and calcite + muscovite/illite mineral groups are the primary carbonate minerals in the subarea (fig 8B–17). The calcite group minerals occur in the fault-bounded central portion of the subarea but are also present in well-defined clusters to the east, and in less well defined patterns in the northern part of the image. Scattered dolomitic minerals occur on the eastern side of the subarea in the Eocene and Pliocene rocks. Iron-bearing carbonates occur along the length of the central fault-bounded region as well as along an east-northeast-trending ridge near lat 68°38′7″E., long 33°12′8″N. that originates within the central fault-bounded region.

8B.3.2.2 Katawas Gold Subarea: Clays and Micas

On the basis of the HyMap data, figure 8B–18 shows the enrichment of clays and micas in the Katawas gold subarea. The subarea is dominated by chlorite and epidote and illite minerals with lesser amounts of muscovite and a very minor amount of montmorillonite. The chlorites and epidotes and illites and montmorillonites occur in rocks of all ages. However, the largest concentration of chlorites and epidotes occurs in Eocene rocks on the western side of the subarea.

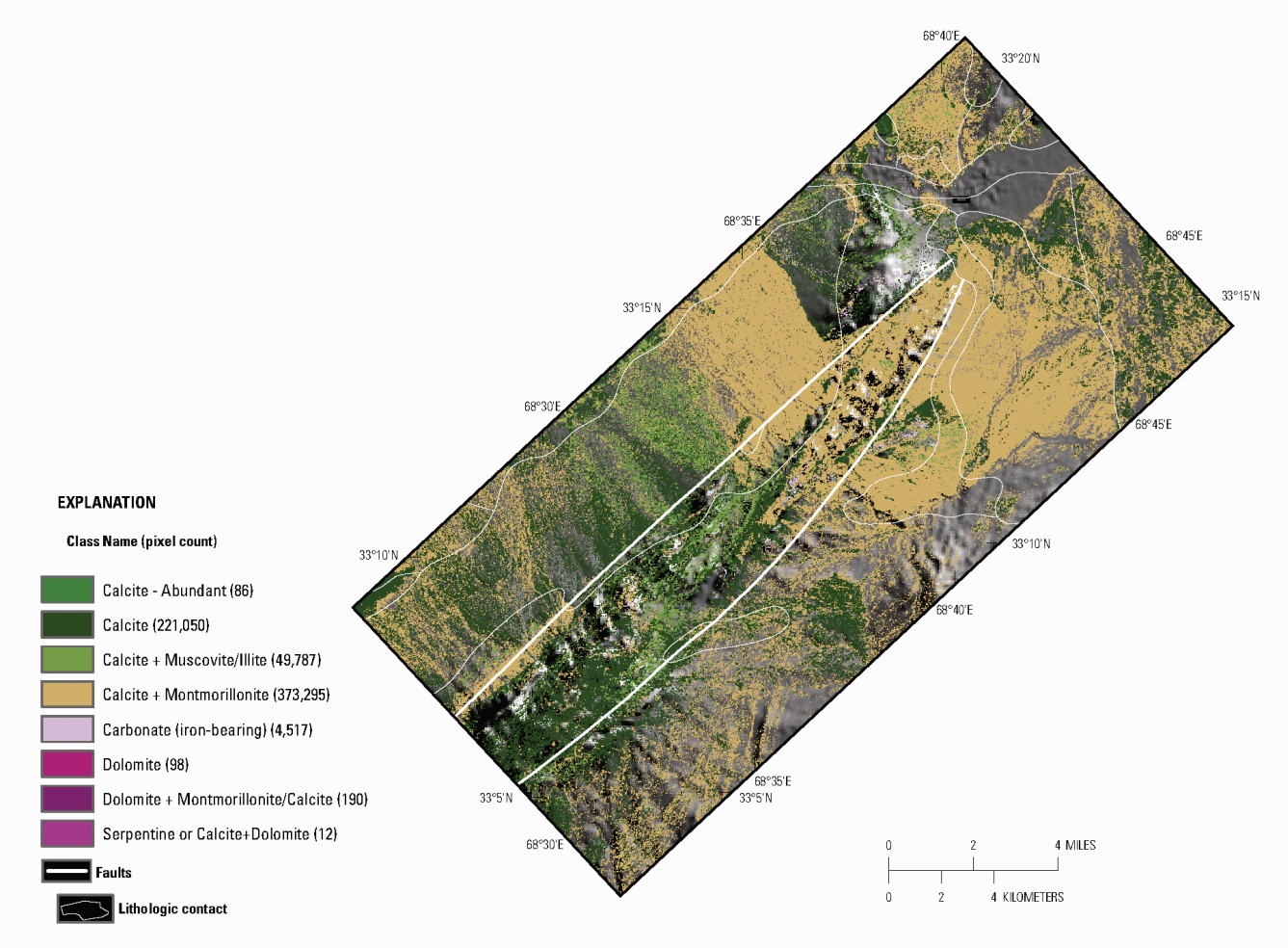

Figure 8B–7. Distribution of carbonate-bearing minerals detected in the HyMap data.

8B.3.2.3 Katawas Gold Subarea: Iron Oxide and Hydroxide Minerals

The central, fault-bounded region and the east-northeast-trending ridge near lat 68°38′7″E., long 33°12′8″N. primarily contain epidote and goethitic minerals (fig. 8B–19) in Paleocene and Eocene rocks. Far less epidote and goethitic minerals are generally present in the younger rock units. However, a well-defined cluster of goethitic minerals ringed by epidote occurs in the northwest part of the image in Pliocene rocks near lat 68°40′E., long 33°16′10″W.

8B.3.2.4 Katawas Gold Subarea: Common Secondary Minerals

The distribution of common secondary minerals (fig. 8B–20) occurs in the central fault-bounded area, the associated east-northeast-trending ridge, and the Eocene rocks adjacent to the fault-bounded central area. Some epidote or chlorite and epidote group minerals are present in the Eocene, late Quaternary, and Recent rocks in the western part of the subarea. Serpentine minerals extend from near lat 68°34′50″E., long 33°9′57″N. to lat 68°38′47″E., long 33°12′9″N. in Paleocene and Eocene rocks. Only a few scattered occurrences of the secondary minerals are seen in rocks younger than Pliocene in the northern part of the subarea.

8B.3.2.5 Katawas Gold Subarea: Common Alteration Minerals

Common alteration materials detected in the HyMap data (fig. 8B–21) for the subarea are chlorite or epidote or Fe-bearing carbonates.

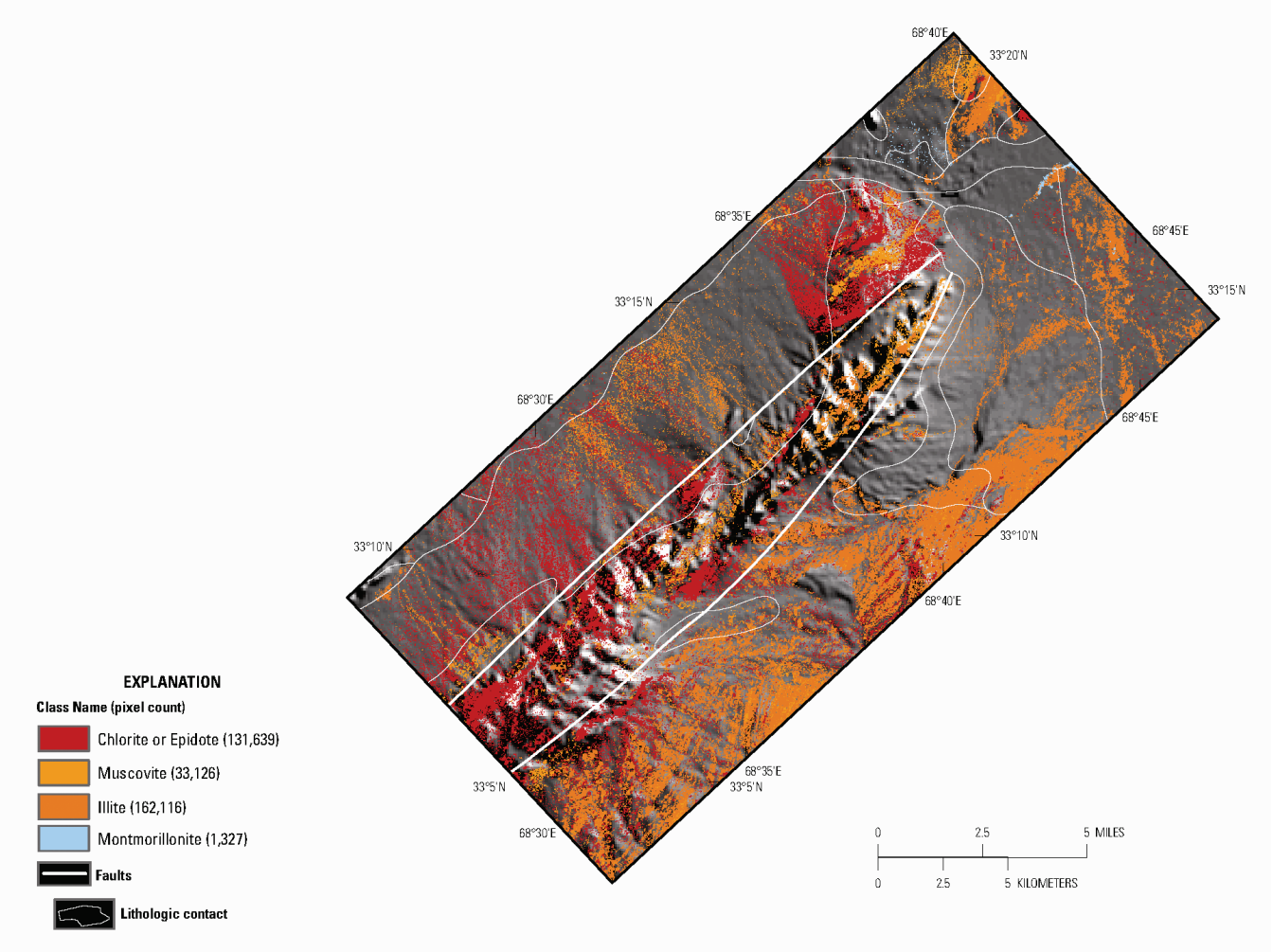

Figure 8B–8. Occurrence of spatially distinct pixels of clays and micas identified in the HyMap data for the Katawas area of interest.

8B.5 Summary

The Katawas AOI and the Katawas gold subarea have no known mineral occurrences. However, the HyMap data for the AOI and subarea show several locations of potential epithermal activity that warrant additional field sampling and geochemical and geophysical studies. Two large areas within the AOI have been identified as anomalous regions and are included in the USGS anomalies report (King, Johnson, and others, 2011).

Large concentrations of chlorite or epidote group minerals and muscovites and illites occur in the southern part (south of approximately lat 33°9′N.) of the AOI (figs. 8B–6, 8B–8; 8B–10; 8B–11) within and adjacent to the central fault-bounded area. Figures 8B–8, 8B–10 and 8B–11 suggest that the chlorite and epidote mineral occurrences may in part be lithologically controlled in bedded rocks. The distribution of muscovites and illites does not appear to be associated with bedded rocks. A small concentration of Fe-bearing carbonates within the muscovites and illites further emphasizes the need for additional studies.

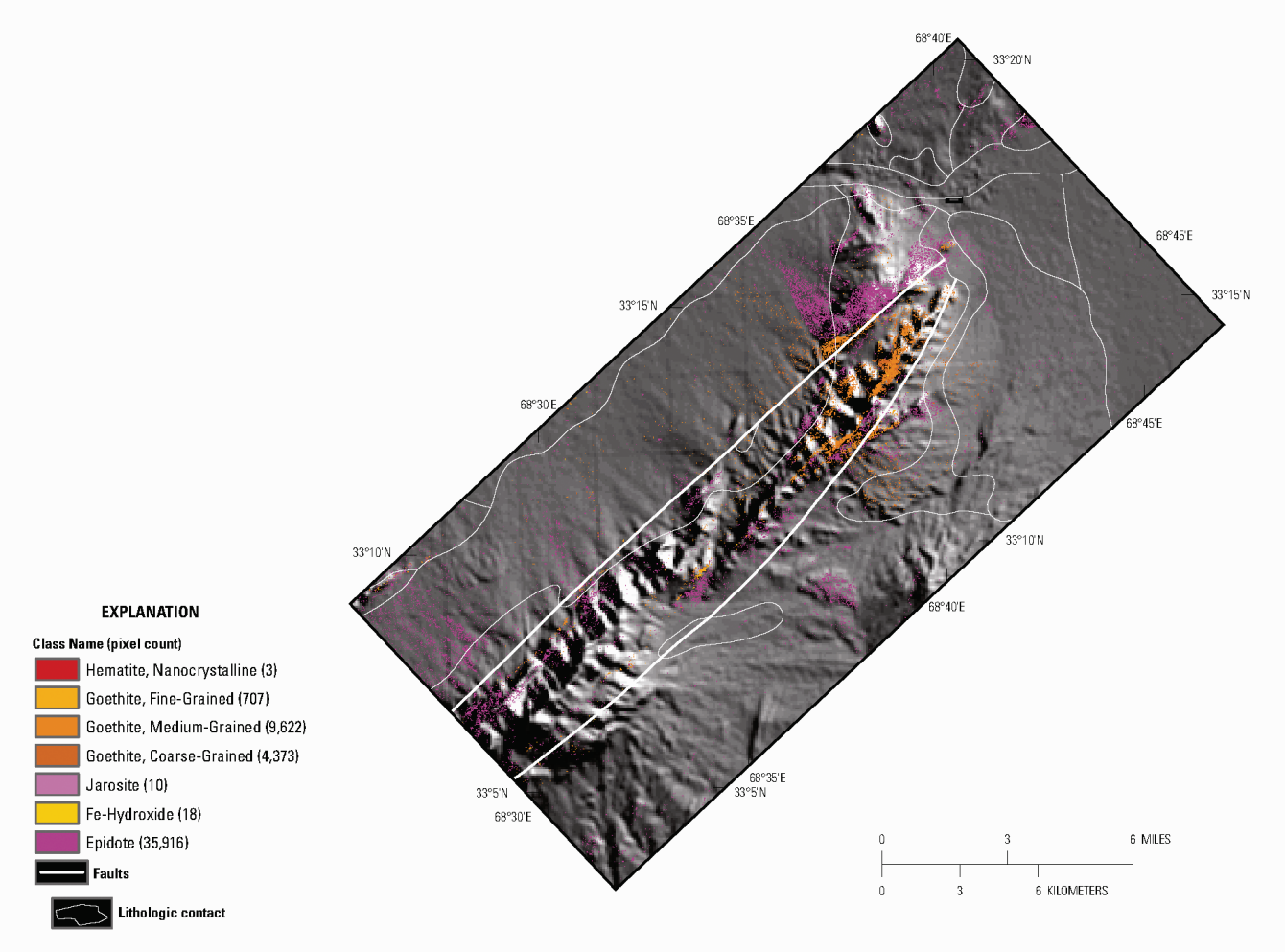

Figure 8B–9. Distribution of Fe-hydroxides and oxides mapped using the HyMap data for the Katawas area of interest.

The Katawas AOI and the Katawas gold subareas both contain Fe^{3+}, Type 1 minerals (figs. 8B–5 and 8B–16) in the northern part of the study areas in rocks ranging in age from Paleocene to Recent. Well-defined clusters of the Fe^{3+}, Type 1 minerals occur in the fault-bounded block in the central portion of the AOI along the northeast-trending linear feature where they occur with a concentration of goethite-rich surficial material. The Fe^{3+}, Type 1 minerals appear to be associated with eroded material (figs 8B–3 and 8B–13) in rocks younger than Paleocene.

A large dark area in the TM data (fig 8B–3) also warrants additional geochemical and geological sampling. The area situated near lat 68°37′28.73″E., long 33°14′48.58″N. shows well-defined clusters of chlorite or epidote, epidote, muscovite, illite, calcite, and Fe-bearing carbonates (figs. 8B–5 to 8B–11). The proximity of the Fe-bearing carbonates and chlorite- and epidote-rich alteration assemblage minerals areas makes the area noteworthy as a potential area of mineralization.

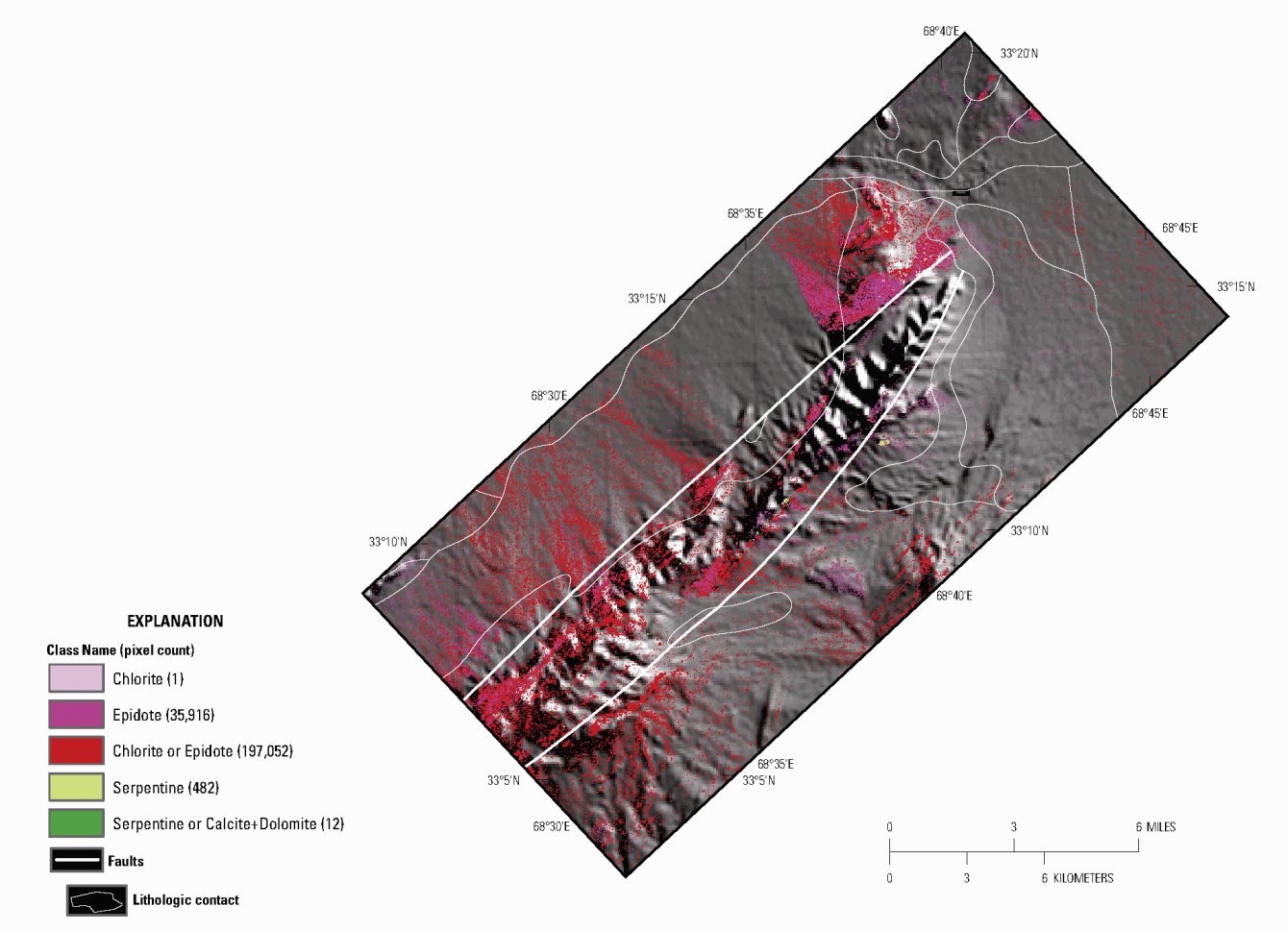

Figure 8B–10. Occurrence and distribution of common secondary minerals detected in the HyMap data.

Previous remote sensing studies using ASTER data (Mars and Rowan, 2007) suggested the potential of mineralization within the Katawas AOI. As in the HyMap data, Bernard Hubbard (written commun., *in* Peters and others, 2007) has also identified (based on ASTER classifications) potential areas of mineralization along a linear trend in the Katawas gold subarea. According to Peters and others (2007), the subarea mineralization occurs within a mercury geochemical halo. The HyMap data for the gold subarea (figs. 8B–15 to 8B–21) best shows the extensive area of alteration along the northeast-trending linear feature and associated east-northeast-trending ridge. The linear feature is primarily in fault-bounded Paleocene rocks. Fe^{2+}-bearing minerals are the dominant surficial material (fig. 8B–16), although large amounts of Fe^{3+}-bearing minerals (discussed above) and chlorite or epidote, epidote, and goethitic minerals are present. Lesser amounts of Fe-bearing carbonate and serpentine pixels are also detected in the area (figs. 8B–15, 8B–17, 8B–20, and 8B–21). Both the Fe-bearing carbonates and serpentine minerals occur in spatially well-defined clusters along the length of the linear feature and associated east-northeast-trending ridge. The detection and association of these phyllic-altered minerals and groups of minerals suggest the possibility of polymetallic copper, gold, and lead deposits (Mars and Rowan, 2007).

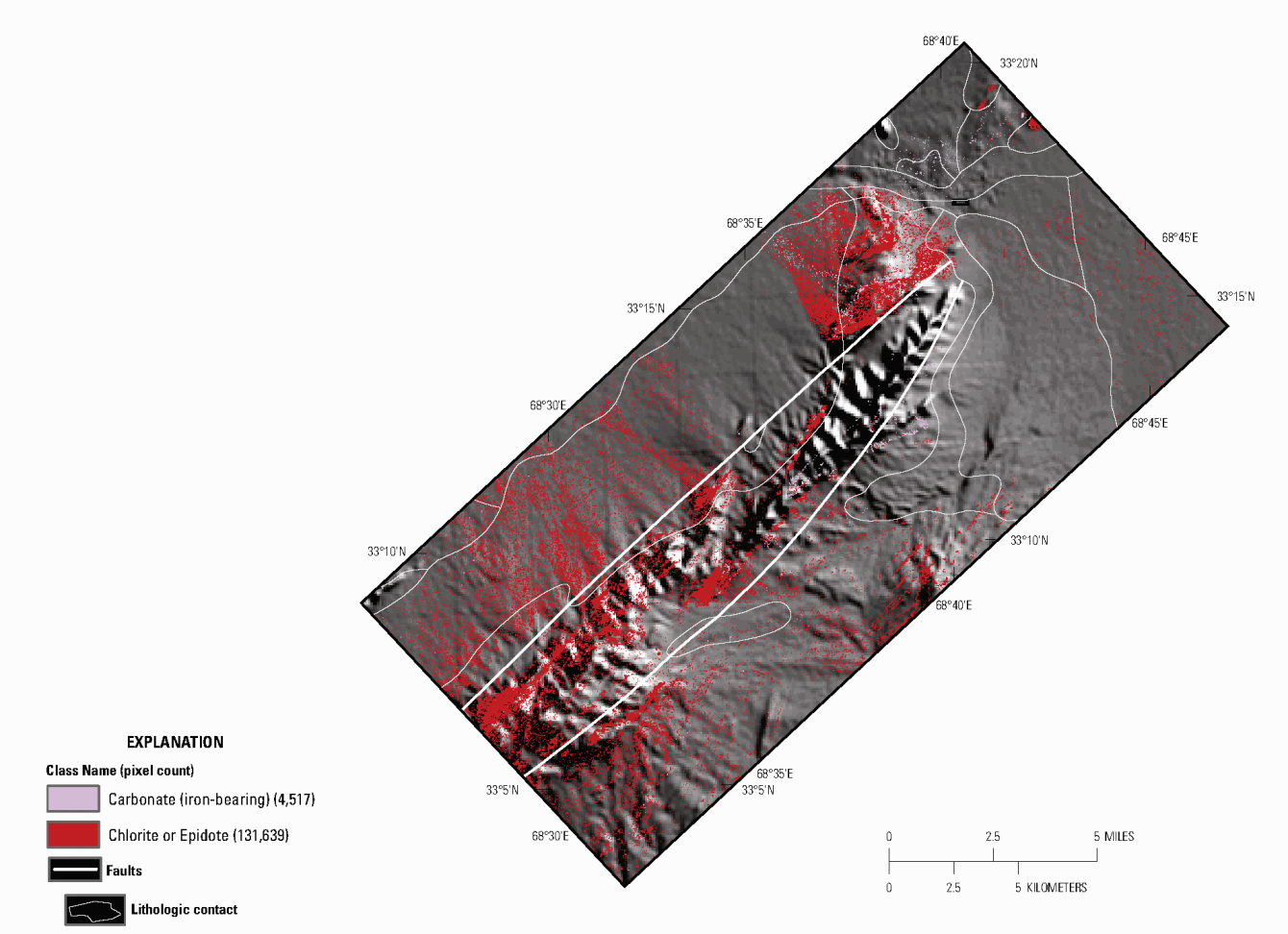

Figure 8B–11. Distribution of common alteration minerals in the Katawas AOI.

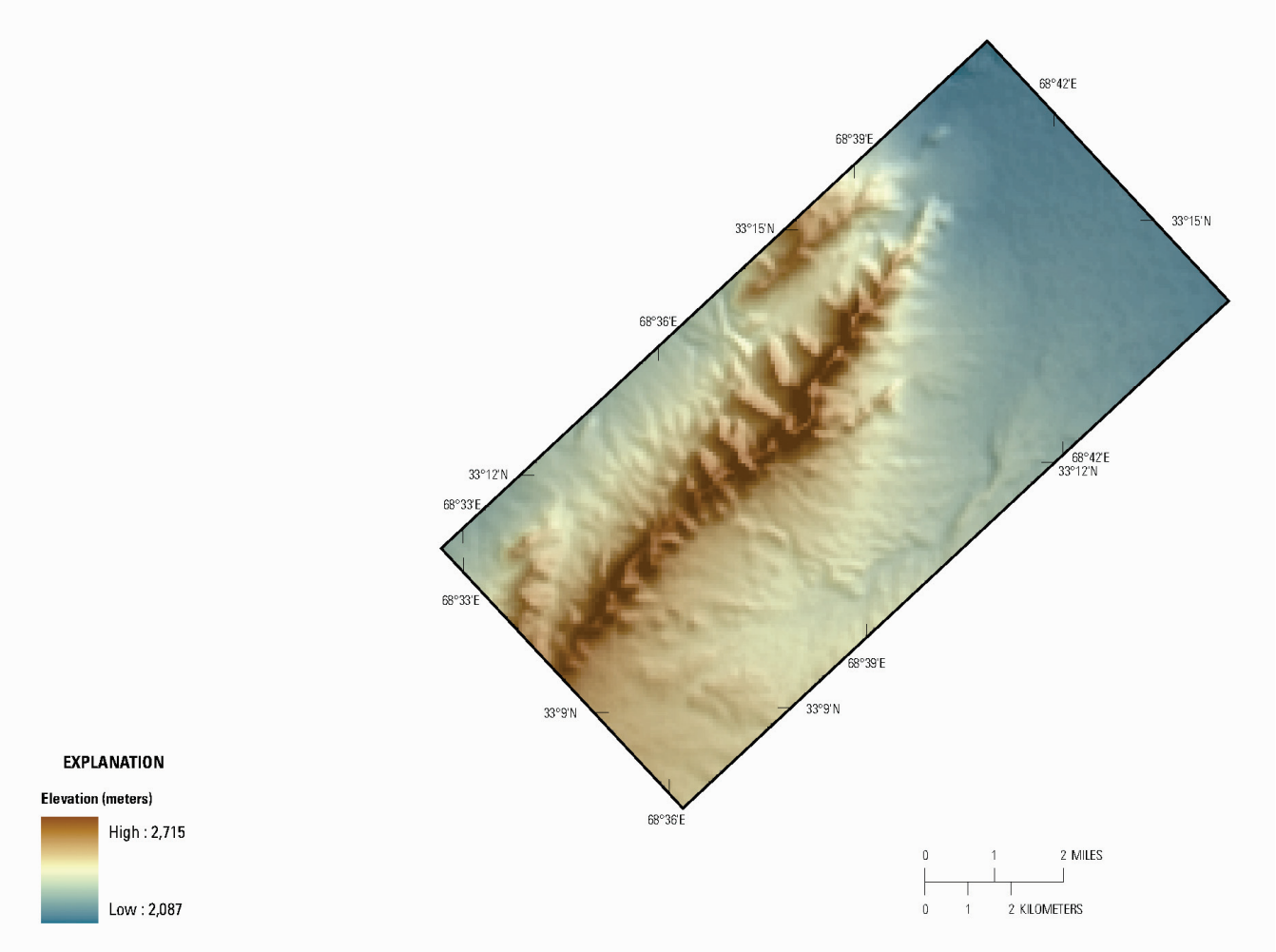

Figure 8B–12. Shaded relief map showing elevation in the Katawas gold subarea. The darker brown tones indicate the higher elevations and the lower elevations are represented by the blue tones.

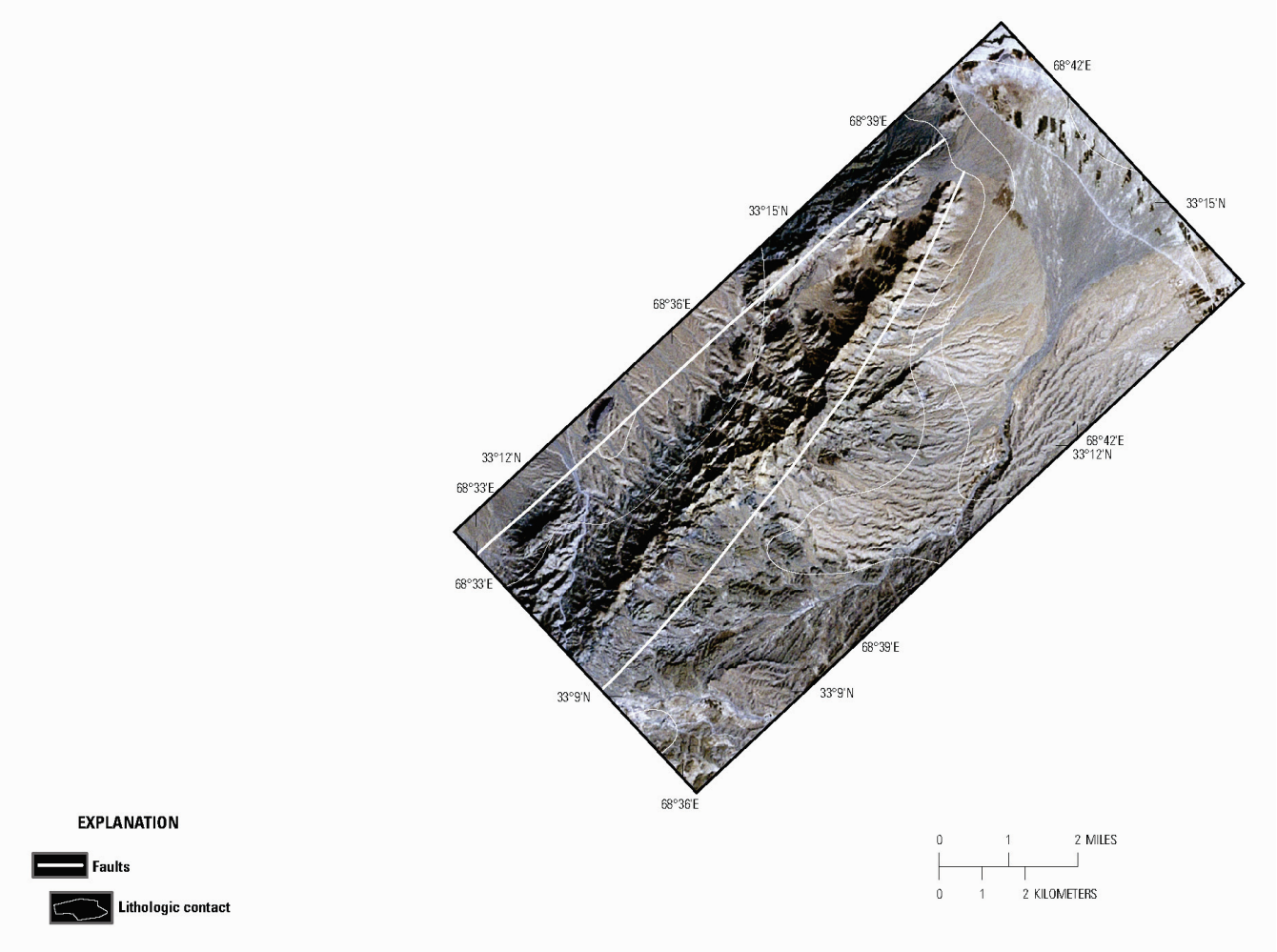

Figure 8B–13. Northeast-striking faults in the Katawas gold subarea. The fault traces (Peters and others, 2007) are placed on a Landsat Enhanced Thematic Mapper (TM) image (Davis, 2007).

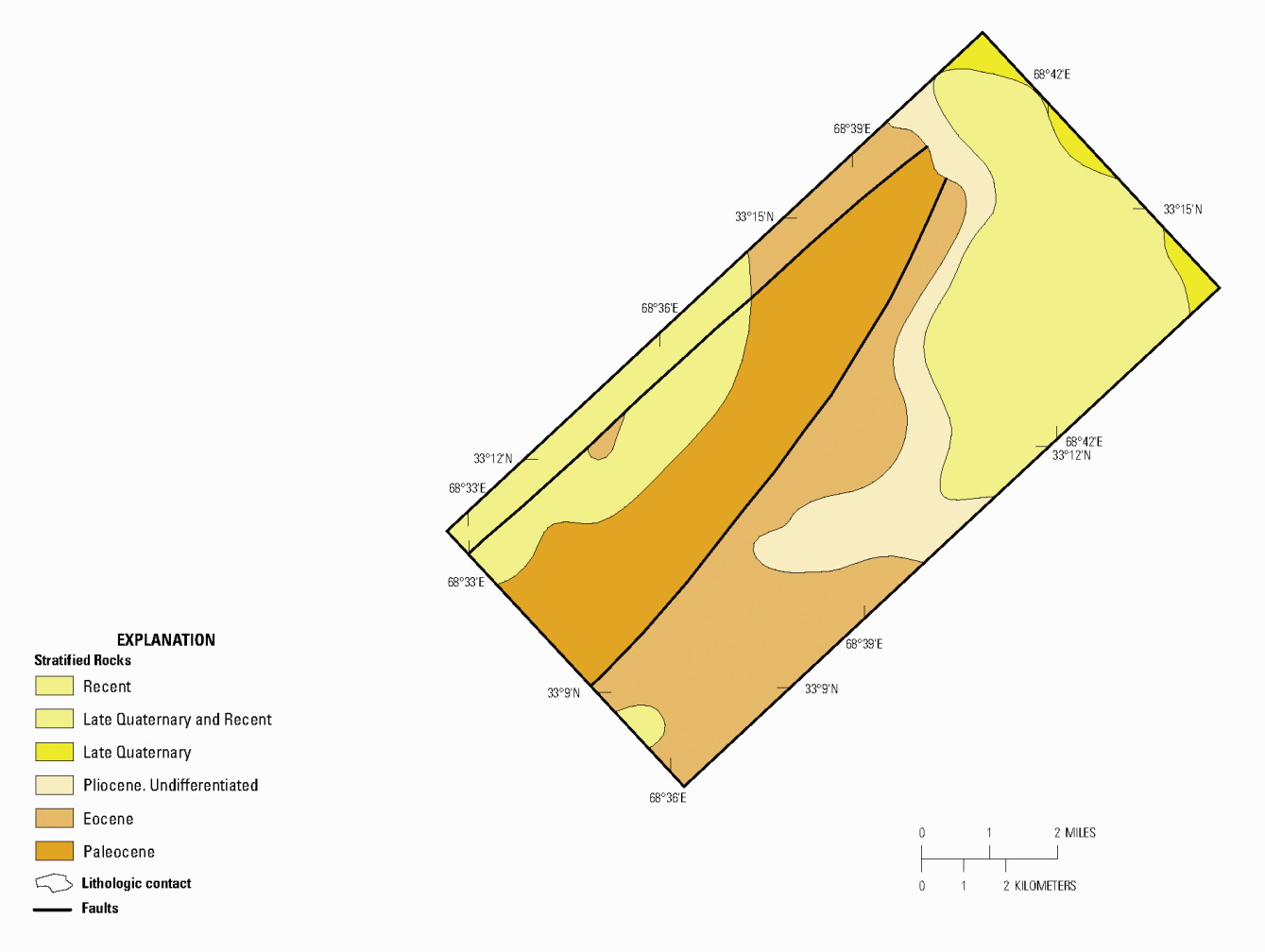

Figure 8B–14. Geologic map of the Katawas gold subarea is from Doebrich and others (2006).

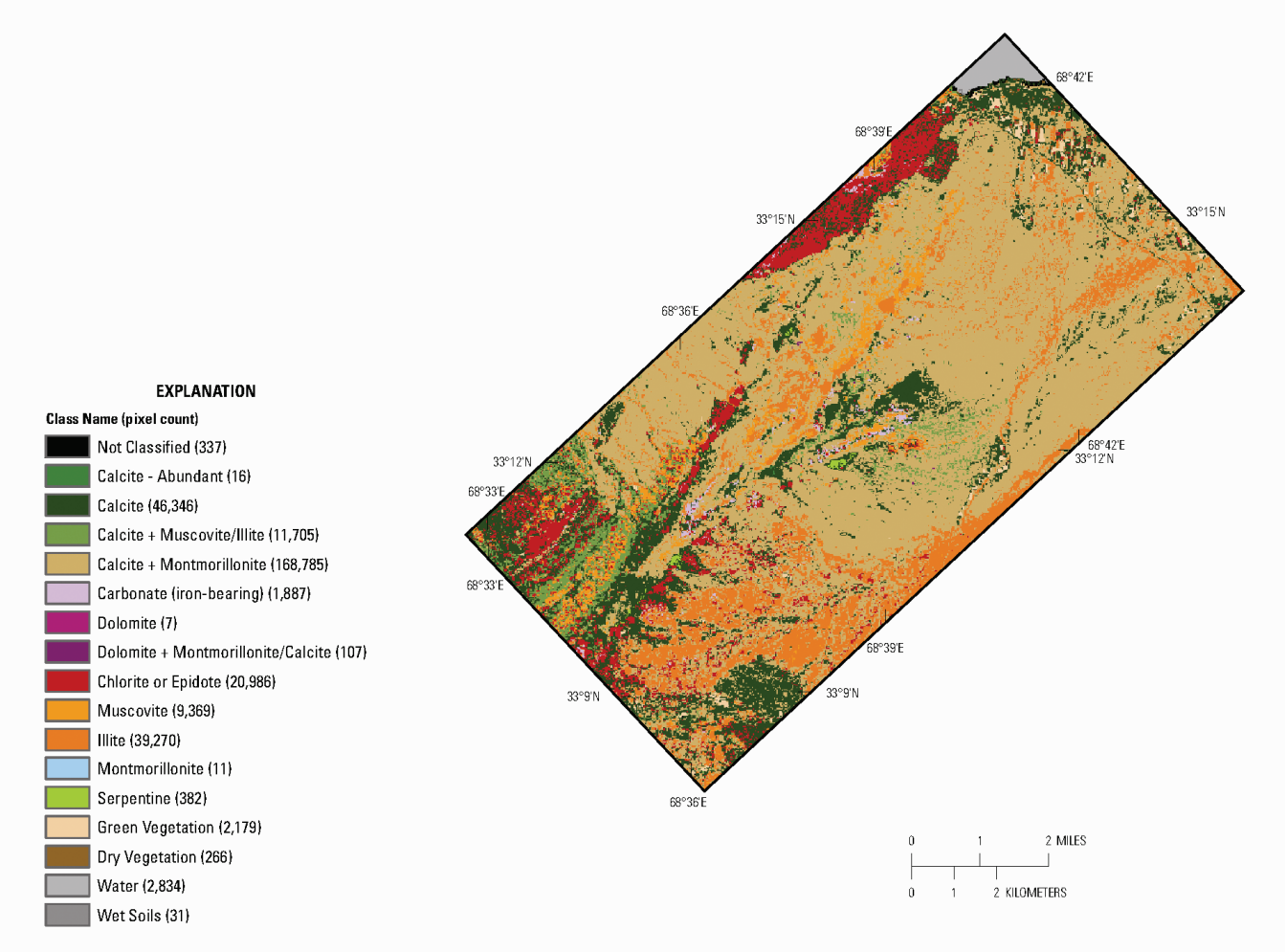

Figure 8B–15. Distribution of clays, carbonates, phyllosilicates, sulphates, and other alteration minerals for the Katawas gold subarea.

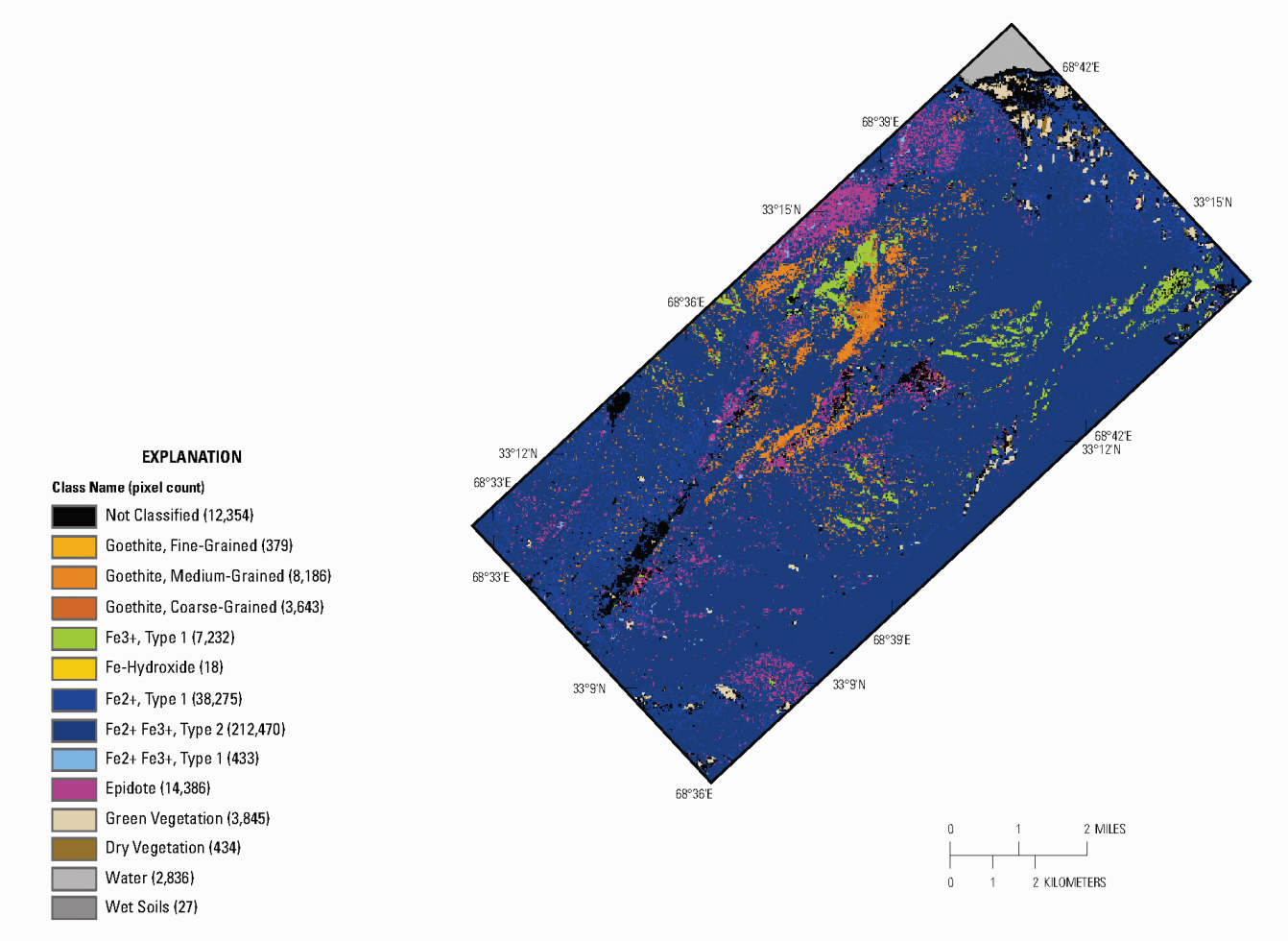

Figure 8B–16. Map showing he iron-bearing and other alteration minerals detected in the HyMap data for the Katawas gold subarea.

Figure 8B–17. Distribution of carbonate-bearing minerals in the Katawas gold subarea detected in the HyMap data.

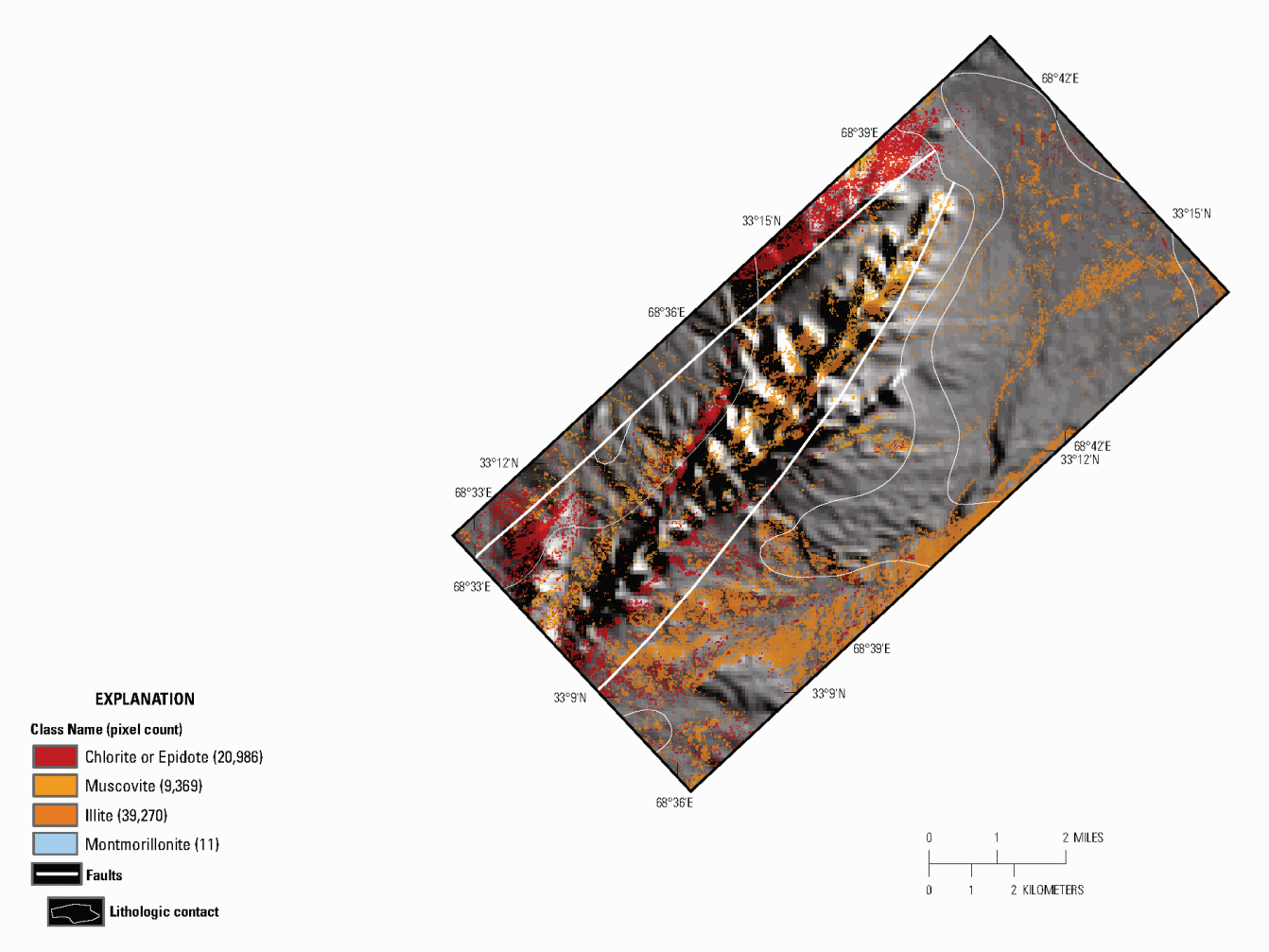

Figure 8B–18. Distribution of clays and micas detected using the HyMap data.

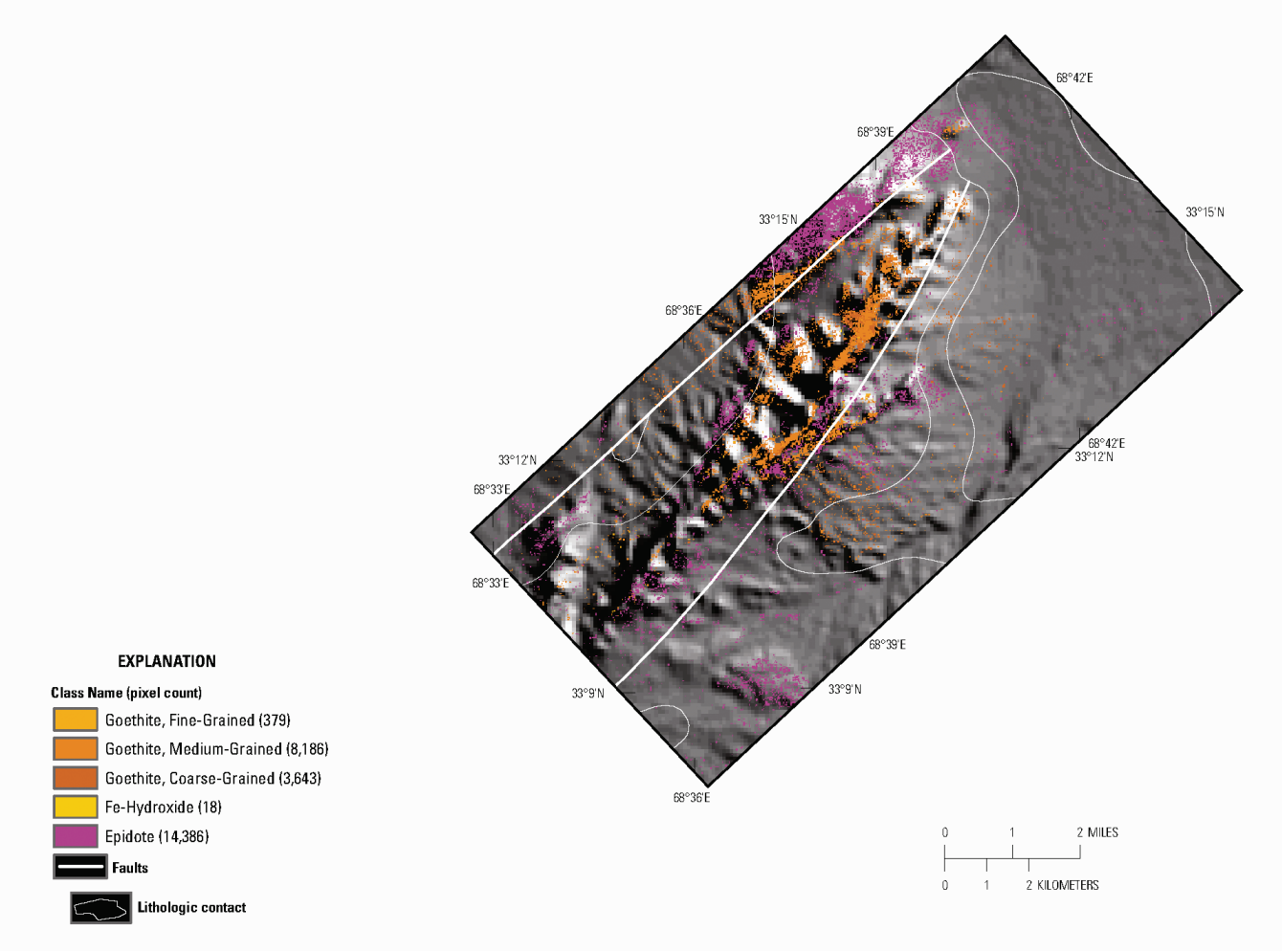

Figure 8B–19. Distribution of Fe-hydroxides and oxides for the Katawas gold subarea.

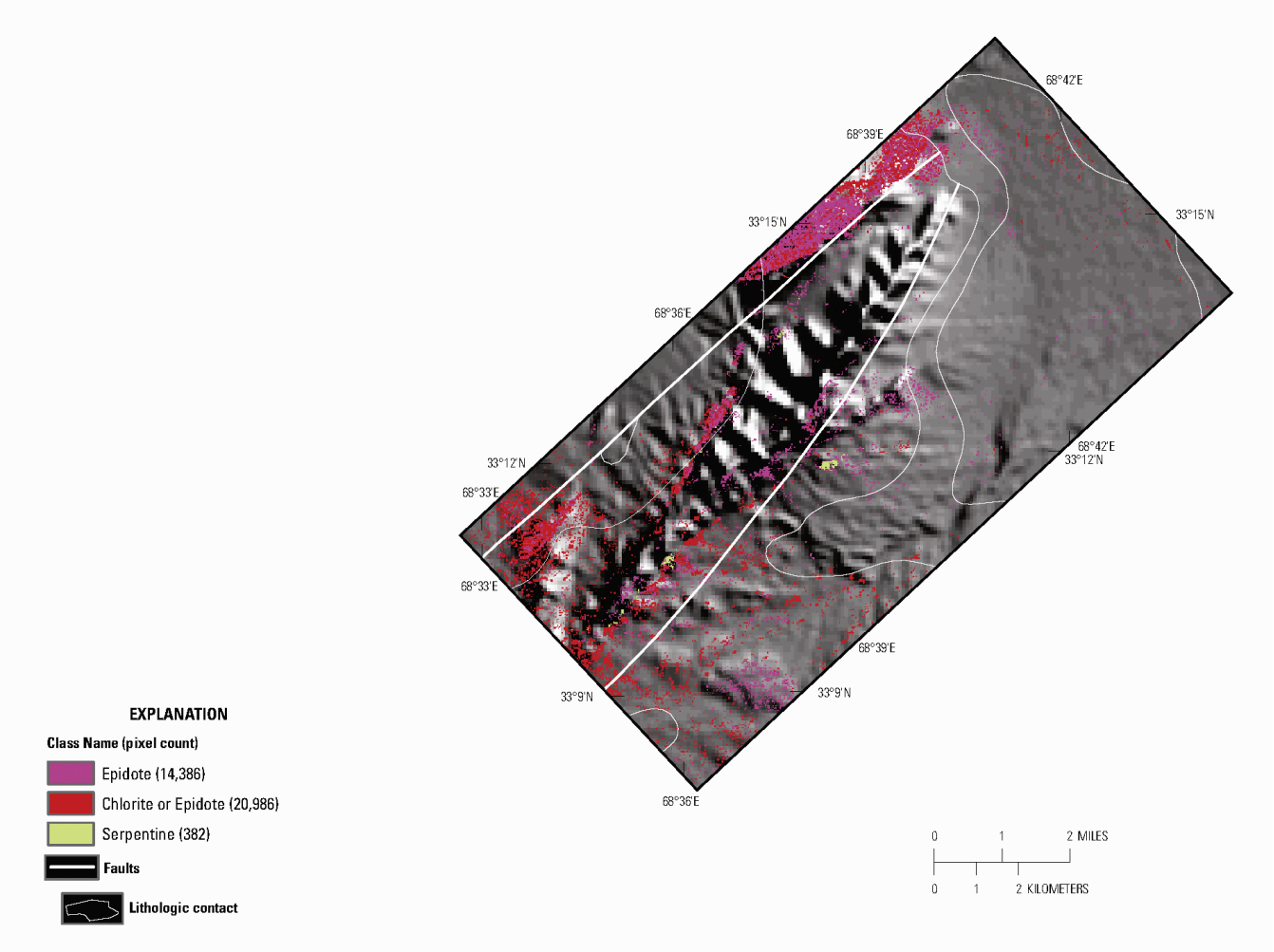

Figure 8B–20. Distribution of common secondary minerals for the Katawas gold subarea.

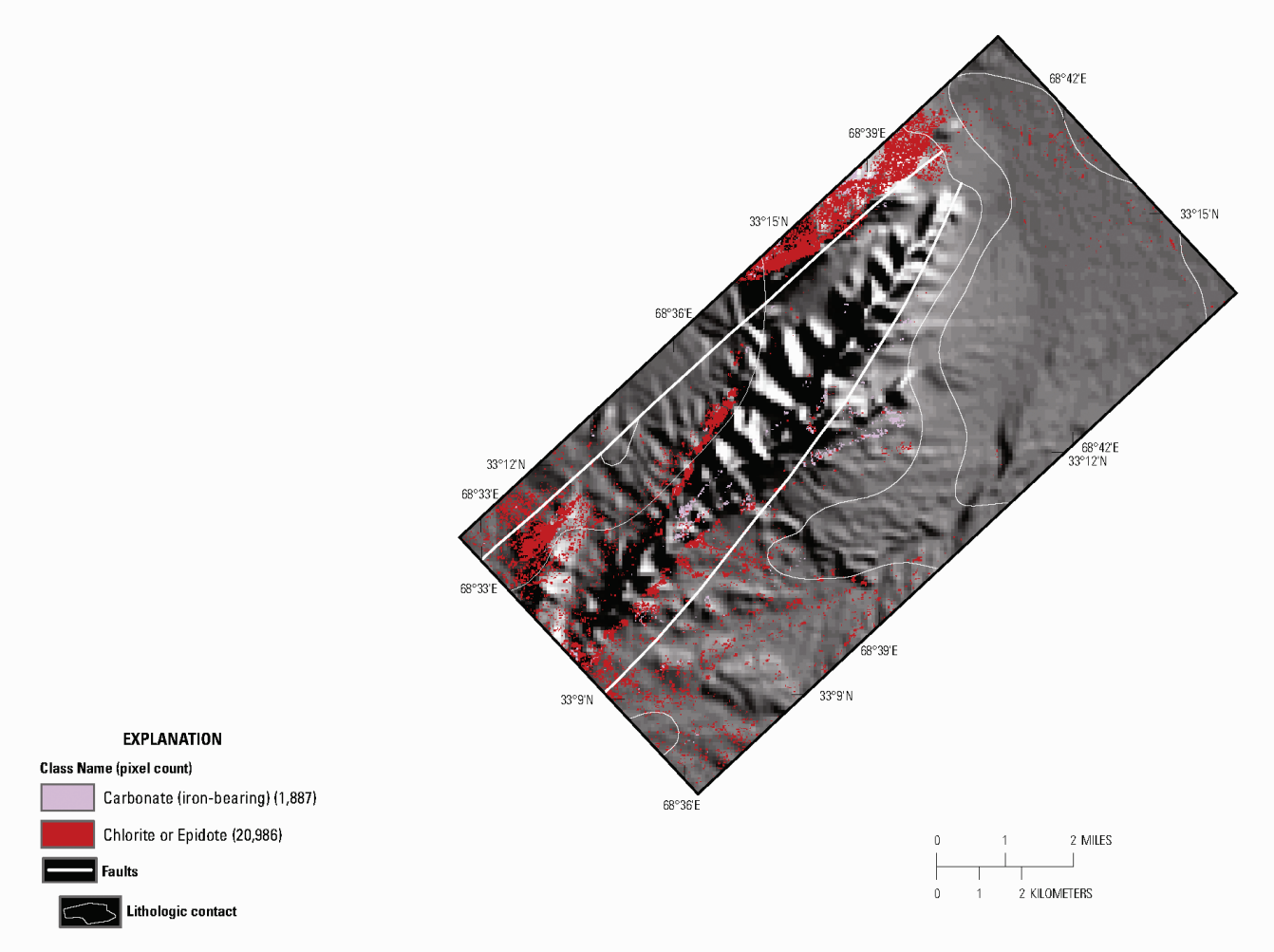

Figure 8B–21. Common alteration materials detected in the HyMap data for the Katawas gold subarea.

8B.6 References Cited

Cocks, T., Jenssen, R., Stewart, A., Wilson, I., and Shields, T., 1998, The HyMap airborne hyperspectral sensor—The system, calibration and performance, *in* Schaepman, M., Schlapfer, D., and Itten, K.I., eds., Proceedings of the 1st EARSeL Workshop on Imaging Spectroscopy, 6–8 October 1998, Zurich: Paris, European Association of Remote Sensing Laboratories, p. 37–43.

Davis, P.A., 2007, Landsat ETM+ false-color image mosaics of Afghanistan: U.S. Geological Survey Open-File Report 2007–1029, 22 p. (Also available at *http://pubs.usgs.gov/of/2007/1029/*.)

Doebrich, J.L., and Wahl, R.R., comps., *with contributions by* Doebrich, J.L., Wahl, R.R., Ludington, S.D., Chirico, P.G., Wandrey, C.J., Bohannon, R.G., Orris, G.J., Bliss, J.D., and _____, 2006, Geologic and mineral resource map of Afghanistan: U.S. Geological Survey Open File Report 2006–1038, scale 1:850,000, available at *http://pubs.usgs.gov/of/2006/1038/*.

Hoefen, T.M., Kokaly, R.F., and King, T.V.V., 2010, Calibration of HyMap data covering the country of Afghanistan, *in* Proceedings of the 15th Australasian Remote Sensing and Photogrammetry Conference, Alice Springs, Australia, September 12–17, 2010, p. 409, available at *http://dl.dropbox.com/u/81114/15ARSPC-Proceedings.zip/*.

King, T.V.V., Kokaly, R.F., Hoefen, T.M., Dudek, K. and Livo, K.E., 2011, Surface materials map of Afghanistan—Iron-bearing minerals and other materials: U.S. Geological Survey Scientific Investigations Map 3152–B.

King, T.V.V., Johnson, M.R., Hoefen, T.M., Kokaly, R.F., and Livo, K.E., 2011, Mapping potential mineral resource anomalies using HyMap data, *in* King, T.V.V., Johnson, M.R., Hubbard, B.E., and Drenth, B.J., eds, Identification of mineral resources in Afghanistan—Detecting and mapping resource anomalies in prioritized areas using geophysical and remote sensing (ASTER and HyMap) data in Afghanistan: U.S. Geological Survey Open-File Report 2011–1229, available at *http://pubs.usgs.gov/of/2011/1229/*.

Kokaly, Ray, 2011, PRISM—Processing routines in IDL for spectroscopic measurements: U.S. Geological Survey Open-File Report 2011–1155, available at *http://pubs.usgs.gov/of/2011/1155/*.

Kokaly, R.F., King, T.V.V., Hoefen, T.M., Dudek, K. and Livo, K.E., 2011, Surface materials map of Afghanistan—Carbonates, phyllosilicates, sulfates, altered minerals, and other materials: U.S. Geological Survey Scientific Investigations Map 3152–A.

Kokaly, R.F., King, T.V.V., and Livo, K.E., 2008, Airborne hyperspectral survey of Afghanistan 2007—Flight line planning and HyMap data collection: U.S. Geological Survey Open-File Report 2008–1235, 14 p.

Mars, J.C., and Rowan, L.C., 2007, Mapping phyllic and argillic-altered rocks in southeastern Afghanistan using advanced spaceborne thermal emission and reflection radiometer (ASTER) data [poster]: U.S. Geological Survey Open-File Report 2007–1006, available at *http://pubs.usgs.gov/of/2007/1006/*.

Peters, S.G., Ludington, S.D., Orris, G.J., Sutphin, D.M., Bliss, J.D., and Rytuba, J.J., eds., and the U.S. Geological Survey-Afghanistan Ministry of Mines Joint Mineral Resource Assessment Team, 2007, Preliminary non-fuel mineral resource assessment of Afghanistan: U.S. Geological Survey Open-File Report 2007–1214, 810 p., 1 CD–ROM. (Also available at *http://pubs.usgs.gov/of/2007/1214/*.)